# 1

# Summary of Trap Properties

## 1.1 Trapping Principles in Paul Traps

Three-dimensional confinement of charged particles requires a potential energy minimum at some region in space, in order that the corresponding force is directed toward that region in all three dimensions. In general, the dependence of the magnitude of this force on the coordinates can have an arbitrary form; however, it is convenient to have a binding force that is harmonic, since this simplifies the analytical description of the particle motion. Thus, we assume

$$F_u = -k_u u, \;\; u = x, y, z. \tag{1.1}$$

It follows from

$$\boldsymbol{F} = -\boldsymbol{\nabla} U, \tag{1.2}$$

where $U = Q\Phi$ is the potential energy, that in general the required function $\Phi$ is a quadratic form in the Cartesian coordinates $x$, $y$, $z$:

$$\Phi = \frac{\Phi_0}{d^2}(Ax^2 + By^2 + Cz^2), \tag{1.3}$$

where $A$, $B$, $C$ are some constants, $d$ a normalizing factor, and $\Phi_0$ can be a time-dependent function. If we attempt to achieve such confinement using an electrostatic field acting on an ion of charge $Q$ we find that to satisfy Laplace's equation $\Delta\Phi = 0$, the coefficients must satisfy $A + B + C = 0$. For the interesting case of rotational symmetry around the $z$-axis, this leads to $A = B = 1$ and $C = -2$ giving the quadrupolar form

$$\Phi = \frac{\Phi_0}{d^2}\,(x^2 + y^2 - 2z^2) = \frac{\Phi_0}{d^2}\,(\rho^2 - 2z^2), \tag{1.4}$$

with $\rho^2 = x^2 + y^2$. Equipotential surfaces are hyperboloids of revolution. If the radial distance from the center ($\rho = z = 0$) of a hyperbolic trap to the ring electrode is called $r_0$, and the axial distance to an end cap is $z_0$, the equations

for the hyperbolic electrode surfaces are

$$\rho^2 - 2z^2 = r_0^2, \qquad (1.5)$$
$$\rho^2 - 2z^2 = -2z_0^2.$$

If the potential difference between the ring and end caps is taken to be $\Phi_0$, then

$$d^2 = r_0^2 + 2z_0^2. \qquad (1.6)$$

From the difference in signs between the radial and axial terms, we see that the potential has a saddle point at the origin, having a minimum along one coordinate but a maximum along the other. Earnshaw's theorem states that it is not possible to generate a minimum of the electrostatic potential in free space. Nevertheless, it is possible to circumvent Earnshaw's theorem by superimposing a magnetic field along the $z$-axis to create what is called the *Penning trap* or to use a time-dependent electric field, leading to the *Paul trap* [1, 2].

The electrodes which create a quadrupole potential consist of three hyperbolic sheets of revolution: A ring electrode and two end caps (Fig. 1.1) which share the same asymptotic cone. The size of the device ranges, in different applications, from several centimeters for the characteristic dimension $d$ to fractions of a millimeter. The trapped charged particles are constrained to a very small central region of the trap.

In recent years, different trap geometries that are easier to manufacture and align and in addition allow better optical access to the trapped particles without further modification have become common; for example, the linear Paul trap which uses four parallel rods as electrodes (Fig. 1.2a). An ac voltage applied between adjacent electrodes leads to dynamical confinement similar to the three-dimensional case, while axial confinement is provided by a static voltage on the end electrodes. For the static Penning trap *cylindrical electrodes* are used (Fig. 1.2b). These electrode geometries produce a harmonic binding force near the center precisely of the classical form. Further away

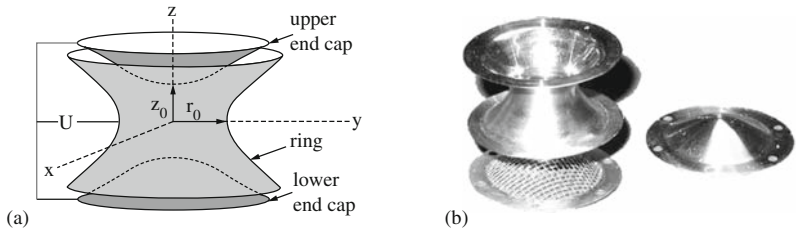


**Fig. 1.1.** Basic arrangement for Paul and Penning traps. The inner electrode surfaces are hyperboloids. The dynamic stabilization in the Paul trap is given by an ac voltage $V_0 \cos \Omega t$. The static stabilization in the Penning trap is given by a dc voltage $U = U_0$ and an axial magnetic field. On the right is a photograph of a trap with $\rho = 1\,\mathrm{cm}$. One of the end caps is a mesh to allow optical access to trapped ions

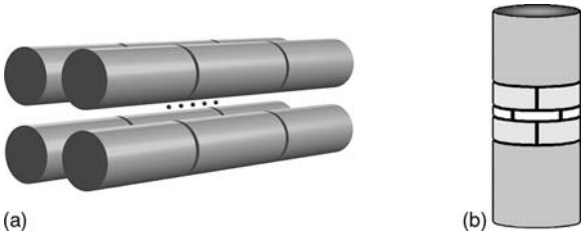


**Fig. 1.2.** Linear Paul trap (**a**) and open end cap cylindrical Penning trap (**b**). A radio-frequency (rf) field applied to the rods of the linear Paul trap confines charged particles in the radial direction, and a dc voltage at the end segments serves for axial trapping. The Penning trap has guard electrodes between the central ring and the end caps to compensate partly for deviations from the ideal quadrupole potential near the trap center. Ion excitation can be performed by rf fields applied to segments of the electrodes

from the origin higher order terms in the expansion of the potential will become significant. For cylindrical Penning traps these can be partially reduced by additional compensation electrodes placed between the ring and end caps as shown in Fig. 1.2b.

### 1.1.1 General Principles

In an ideal Paul trap an oscillating electric potential usually in combination with a static component, $U_0 + V_0 \cos \Omega t$, is applied between the ring and the pair of end cap electrodes. It creates a potential of the form

$$\Phi = \frac{U_0 + V_0 \cos \Omega t}{2d^2}(\rho^2 - 2z^2). \tag{1.7}$$

Since the trapping field is inhomogeneous, the average force acting on the particle, taken over many oscillations of the field, is not zero. Depending on the amplitude and frequency of the field, the net force may be convergent toward the center of the trap leading to confinement, or divergent leading to the loss of the particle. Thus, although the electric force alternately causes convergent and divergent motions of the particle in any given direction it is possible by appropriate choice of field amplitude and frequency, to have a time-averaged restoring force in all three dimensions toward the center of the trap as required for confinement [3]. The conditions for stable confinement of an ion with mass $M$ and charge $Q$ in the Paul field may be derived by solving the equation of motion

$$\frac{\mathrm{d}^2 u}{\mathrm{d}t^2} = \frac{Q}{Md^2}(U_0 + V_0 \cos \Omega t)u, \;\; u = x, y, z. \tag{1.8}$$

Using the dimensionless parameters $a_x = a_y = -2a_z = -4QU_0/(Md^2\Omega^2)$ and $q_x = q_y = 2q_z = 2QV_0/(Md^2\Omega^2)$, we obtain a system of three differential

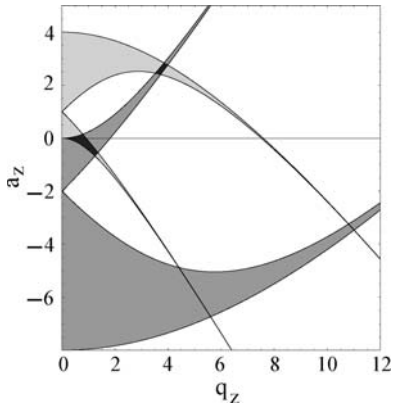


**Fig. 1.3.** The stability domains for the ideal Paul trap. *Light gray*: $z$-direction; *dark gray*: $r$-direction. Three-dimensional stability is assured in the overlapping regions

equations of the homogeneous Mathieu type [4, 5]

$$\frac{\mathrm{d}^2u}{\mathrm{d}\tau^2} + (a - 2q\cos 2\tau)u = 0, \tag{1.9}$$

where $\tau = \Omega t/2$. The values of $a$ and $q$ for which the solutions are stable simultaneously for both directions, an obvious requirement for three-dimensional confinement, are found by using the relationships $a_z = -2a_r$, $q_z = 2q_r$ to make a composite plot of the boundaries of stability for both directions on the same set of axes: The overlap regions lead to three-dimensional confinement (Fig. 1.3). The most important for practical purposes is the stable region near the origin which has been exclusively used for ion confinement.

The stable solutions of the Mathieu equation can be expressed in the form of a Fourier series, thus

$$u_i(\tau) = A_i \sum_{n=-\infty}^{\infty} c_{2n}\cos(\beta_i + 2n)\tau + B_i \sum_{n=-\infty}^{\infty} c_{2n}\sin(\beta_i + 2n)\tau, \tag{1.10}$$

where $A_i$ and $B_i$ are constants depending on the initial conditions. The stability parameters $\beta_i$ are functions of $a_i$ and $q_i$. The coefficients $c_{2n}$, which are the amplitudes of the Fourier components of the particle motion, decrease with increasing $n$. For small values of $a_i$, $q_i \ll 1$, we can approximate the stability parameter $\beta_i$ by

$$\beta_i^2 \simeq a_i + \frac{q_i^2}{2},\ i = \rho, z. \tag{1.11}$$

In this so-called *adiabatic approximation* only the coefficients $c_{2n}$ with $n = 1$ giving $c_{-2} = c_{+2} = -(q_i/4)c_0$ are considered, and the other with $n \geq 2$ are neglected. The ion motion simplifies to

$$u_i(t) = A\left(1 - \frac{q_i}{2}\cos\Omega t\right)\cos\omega_i t, \tag{1.12}$$

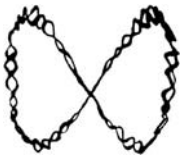

**Fig. 1.4.** Observed trajectory of a microparticle in a Paul-type trap [6]

with

$$\omega_i = \beta_i \Omega/2. \tag{1.13}$$

This can be considered as the motion of an oscillator of frequency $\omega$ whose amplitude is modulated with the trap's driving frequency $\Omega$. Since it is assumed that $\beta \ll 1$, the oscillation at $\omega$, usually called the secular motion or macromotion, is slow compared with the superimposed fast micromotion at $\Omega$. Because of the large difference in the frequencies $\omega$ and $\Omega$, the ion motion can be well separated into two components and the behavior of the slow motion at frequency $\omega$ can be considered as separate, while time averaging over the fast oscillation at $\Omega$. Wuerker et al. [6] have taken photographs of single particle trajectories of microparticles in a Paul-type trap at low frequencies of the trapping field demonstrating the validity of this approximation (Fig. 1.4).

### 1.1.2 Potential Depth

In the adiabatic approximation, an expression for the depth of the confining potential can be derived by considering the secular motion only. The ion behaves in the axial direction as a harmonic oscillator of frequency $\omega_z$. For no dc voltage ($a = 0$) we have

$$\omega_z = \frac{QV_0}{\sqrt{2}Mz_0^2\Omega}. \tag{1.14}$$

This corresponds to a time-averaged (pseudo)potential of depth in the axial direction of

$$\bar{D}_z = \frac{QV_0^2}{4Mz_0^2\Omega^2}, \tag{1.15}$$

and similarly in the radial direction

$$\bar{D}_r = \frac{QV_0^2}{4Mr_0^2\Omega^2}. \tag{1.16}$$

For $r_0^2 = 2z_0^2$ we have $\bar{D}_r = \bar{D}_z/2$.

The effect of an additional dc voltage on the trap electrodes is to alter the depth of the potential in the field direction. If the voltage $U_0$ is applied symmetrically to the trap electrodes (that is, the trap center is at zero potential),

we have

$$\begin{aligned} \bar{D}'_{\mathrm{z}} &= \bar{D}_z + U_0/2, \\ \bar{D}'_{\mathrm{r}} &= \bar{D}_{\mathrm{r}} - U_0/2. \end{aligned} \tag{1.17}$$

A typical value for a trap of 1 cm radius $r_0$ driven by 500 V at a frequency of $\Omega/2\pi = 1\,\mathrm{MHz}$ and an ion atomic mass of 100 is 25 eV for the radial potential depth.

### 1.1.3 Motional Spectrum

Equation (1.10) shows that the motional spectrum contains the frequencies $(\beta_i + 2n)\Omega/2$, where $n$ is an integer having the fundamental frequencies given by $n = 0$. To experimentally demonstrate this spectrum, the motion can be excited by an additional (weak) radio-frequency (rf) field applied to the electrodes. When resonance occurs between the detection field frequency and one of the frequencies in the ion spectrum, the motion becomes excited and some ions may leave the trap, providing a signal commensurate with the number of trapped ions. Figure 1.5 shows an example where a cloud of stored $N_2{}^+$ ions is excited at the motional resonances occurring at the frequencies predicted by theory.

### 1.1.4 Optimum Trapping Conditions

If we define the optimum trapping conditions for a Paul trap as those which yield the highest density of trapped particles, we are faced with conflicting requirements: On one hand, the maximum trapped ion number increases with

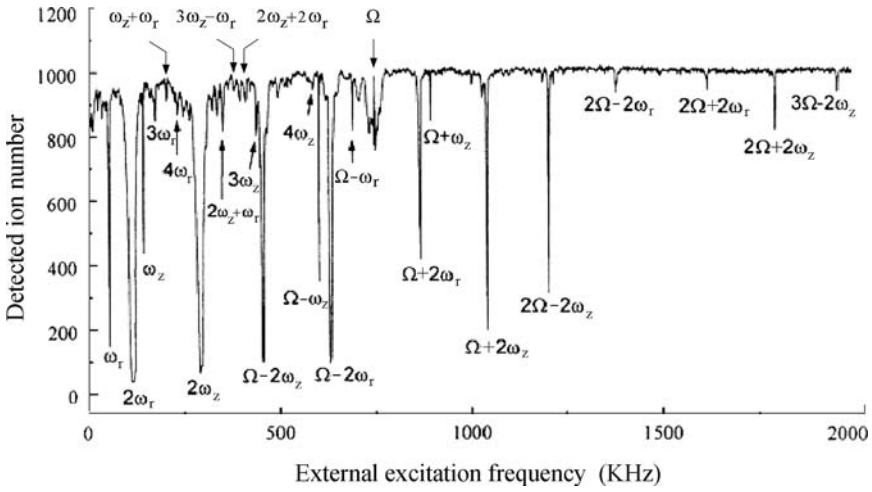


**Fig. 1.5.** Motional resonances of a $N_2{}^+$ cloud in a quadrupole Paul trap [7]

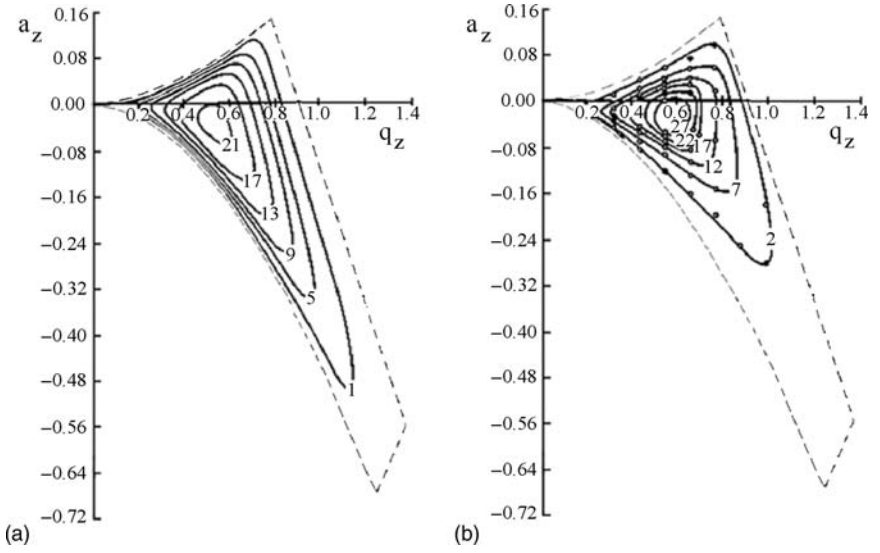


**Fig. 1.6.** Optimum trapping conditions. (**a**) Computed lines of equal ion density within the stability diagram. The numbers give relative densities. (**b**) Experimental lines of equal ion density from laser-induced fluorescence [8]

the potential depth $D$, since the number is limited by the condition that the space charge potential of the ions not exceed $D$. On the other hand, the oscillation amplitudes also increase at the same time, resulting in increasing ion loss for higher $q$ in a trap of a given size. Consequently the maximum ion number is expected in a region around the center of the stability diagram. This has been confirmed experimentally by systematic variation of the trapping parameters and a measurement of the relative trapped ion number by laser induced fluorescence (Fig. 1.6) [8].

### 1.1.5 Storage Time

Once the ions are stored in a Paul trap they would remain there in the ideal case for an infinitely long time. In practice, the storage time may be limited by trap imperfections as discussed later. Their effects can be avoided by proper choice of the operating conditions. The limiting factor then would be collisions with neutral background molecules. Thus, operation of the traps in ultra-high vacuum is necessary; in fact at pressures around $10^{-8}$ Pa storage times of many hours are routinely obtained.

Under certain conditions, however, higher background pressure may have a beneficial effect on the storage time as well. Major and Dehmelt [9] have pointed out that ion–neutral collisions lead to damping of the ion motion and thus to increased storage times when the ion mass exceeds the mass of the neutral atom or molecule. This has been experimentally verified in many cases

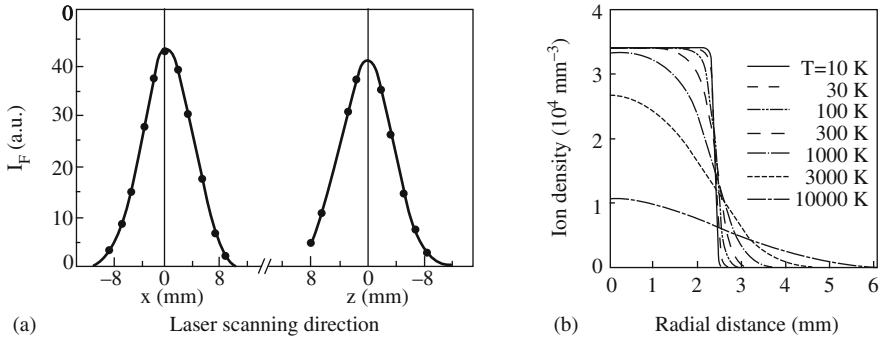


**Fig. 1.7.** (**a**) Fluorescence $I_F$ of $Ba^+$ ions in axial and radial direction in a Paul trap of 4 cm ring radius showing a Gaussian density distribution [10]. (**b**) Calculated density distributions for different ion temperatures [11]

and storage times of many days for heavy ions such as $Ba^+$ or $Pb^+$ have been obtained when operating with light buffer gases (He, $N_2$, Ne) at pressures as high as $10^{-2}$ Pa.

### 1.1.6 Ion Density Distribution

In thermal equilibrium at high temperatures a cloud of trapped ions assumes a Gaussian density distribution, averaged over a period of the micromotion. This has been experimentally confirmed by scanning a laser spatially through the trap and observing the fluorescence light induced by laser exitation (Fig. 1.7). When the ion temperature is lowered, the cloud diameter shrinks until a homogeneously charged sphere is obtained. From the width of the distribution the ions' average kinetic energy can be derived [10]. As a rule of thumb, it amounts to 1/10 of the potential depth.

### 1.1.7 Storage Capability

The maximum density $n$ of ions that can be stored occurs when the space charge potential created by the ion cloud, given by $\nabla^2 V_{sc} = Qn/\varepsilon_0$ with $\varepsilon_0$ the permittivity of free space, equals the trap potential depth. For a spherical potential shape $n$ is given by

$$n = \frac{3\varepsilon_0 \bar{D}}{Qr_0^2}. \tag{1.18}$$

The total stored ion number $N$ follows from integration over the active trap volume. Taking a density distribution as shown in Fig. 1.7 we arrive at a maximum ion number $N \simeq 10^6$ in fair agreement with observations.

### 1.1.8 Paul Trap Imperfections

A single ion in a perfect quadrupole potential does not describe a real experimental situation. Truncations of the electrodes, misalignments, or machining errors change the shape of the potential field. The equations of motion as discussed earlier are valid only for a single confined particle. Simultaneous confinement of several particles requires the consideration of space charge effects. For a low density cloud it seems reasonable to assume that the particles move in somewhat modified orbits, mainly independent of each other except for rare Coulomb scattering events. These collisions ultimately serve to establish a thermal equilibrium between the particles. They may be considered as small perturbations to the particle motion, provided the time average of the Coulomb interaction potential is small compared to the average energy of the individual particle. Then the particle cloud may be described as ideal gas of noninteracting particles in thermal equilibrium.

Deviations of the trap potential from the ideal quadrupolar form can be treated by a series expansion in spherical harmonics, thus

$$\Phi(\rho,\theta) = (U_0 + V_0 \cos \Omega t) \sum_{n=2}^{\infty} c_n \left(\frac{\rho}{d}\right)^n P_n(\cos\theta), \tag{1.19}$$

where $P_n(\cos\theta)$ are the Legendre polynomials of order $n$. For rotational and mirror symmetry the odd coefficients $c_n$ vanish. The terms beyond the quadrupole ($c_2$) may be looked on as perturbing potentials the lowest of which is the octupole ($c_4$), followed by the dodecapole ($c_6$). The equations of motion for a single particle in an imperfect Paul trap now become coupled inhomogeneous differential equations which cannot be solved analytically. It has been shown, however, that, under certain conditions that would otherwise give stability in a perfect quadrupole field, the motion becomes unstable [12, 13]. These conditions can be expressed in terms of the stability parameters $\beta_r$ and $\beta_z$, thus

$$n_r\beta_r + n_z\beta_z = 2k, \tag{1.20}$$

or equivalently

$$n_r\omega_\mathrm{r} + n_z\omega_\mathrm{z} = k\Omega, \tag{1.21}$$

where $n_r$, $n_z$, $k$ are integers. This relationship states that if a linear combination of harmonics of the ion macrofrequencies coincides with a harmonic of the high-frequency trapping field, an ion will gain energy from that field until it gets lost from the trap.

Experimental proof of the instabilities has been obtained by measurements of the number of trapped ions at different operating points. A high-resolution scan of the stability diagram was given by Alheit et al. [14], who observed instabilities resulting from very high orders of perturbing potentials (Fig. 1.8). From this figure it is evident that strong instabilities occur at the high-$q$ region of the stability diagram, due to hexapole and octupole terms in the expansion

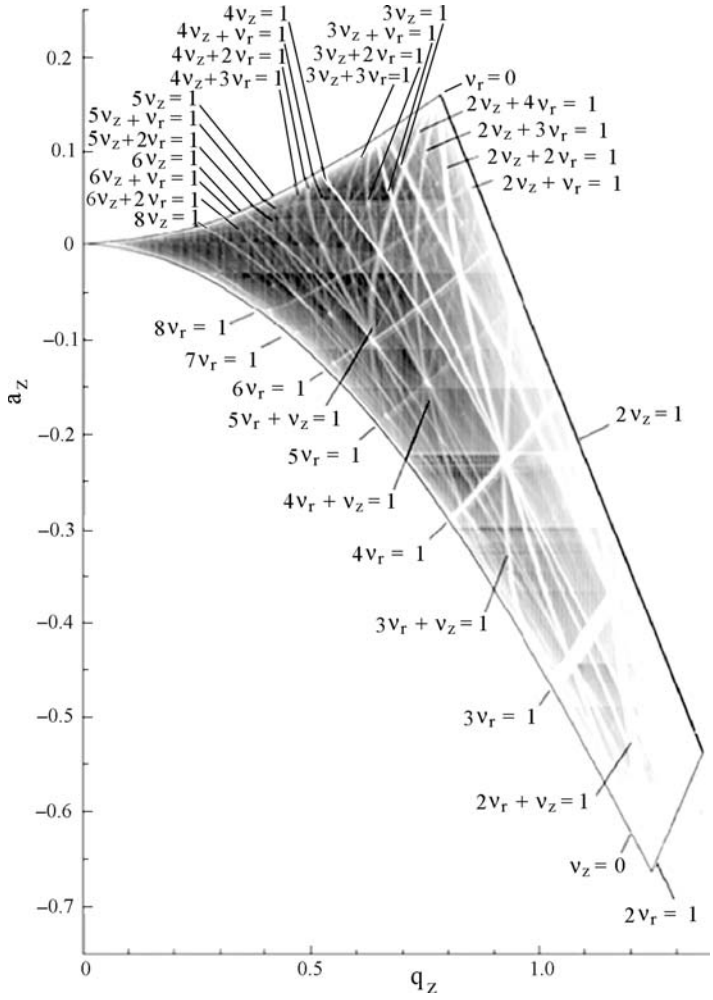


**Fig. 1.8.** Experimentally observed lines of instabilities in the first region of stability of a real Paul trap taken with $H_2{}^+$ ions. The unstable lines are assigned according to (1.21). The intensity in *gray* is proportional to the trapped ion number [14]

of the potential, which are the highest orders expected in a reasonably well machined trap. This makes it very difficult to obtain long storage times at high amplitudes of the trapping voltage (for a given frequency). In fact, the most stable conditions are obtained for small $q$ values near the $a = 0$ axis; here the instability condition on the frequencies is met only for a very high-resonance order which would occur only if the field was highly imperfect.

As another consequence of the presence of the higher order terms in the trapping potential, the motional eigenfrequencies are shifted with respect to the pure quadrupole field, and moreover in an amplitude dependent way.

These shifts are of particular importance in the case of Penning traps, when they are used for very high-resolution mass spectrometry, and will be discussed later. While for the ideal harmonic potential the line shape of the resonances is a Lorentzian, it now becomes asymmetric. From a theoretical fit to the line shape the size of the higher order coefficients in the series expansion of the potential (1.20) can be determined [15]. In addition to the ideal case the motional spectrum now contains not only the eigenfrequencies as calculated from (1.10) but also the sum and difference frequencies.

## 1.2 Trapping Principles in Penning Traps

### 1.2.1 Theory of the Ideal Penning Trap

The Penning trap uses static electric and magnetic fields to confine charged particles. The ideal Penning trap is formed by the superposition of a homogeneous magnetic field $\boldsymbol{B} = (0, 0, B_0)$ and an electric field $\boldsymbol{E} = \boldsymbol{\nabla}\Phi$ derived from the quadrupole potential as given in (1.4).

A particle of mass $M$, charge $Q$, and velocity $\boldsymbol{v} = (v_x, v_y, v_z)$ moving in the fields $\boldsymbol{E}$ and $\boldsymbol{B}$ experiences a force

$$\boldsymbol{F} = -Q\boldsymbol{\nabla}\Phi + Q(\boldsymbol{v} \times \boldsymbol{B}). \tag{1.22}$$

Since the magnetic field is along the $z$-axis, the $z$ component of the force is purely electrostatic, and therefore to confine the particle in the $z$-direction we must have $QU_0 > 0$. The $x$- and $y$-components of $\boldsymbol{F}$ are a combination of a dominant restraining force due to the magnetic field, characterized by the cyclotron frequency

$$\omega_\mathrm{c} = \frac{|QB_0|}{M}, \tag{1.23}$$

and a repulsive electrostatic force that tries to push the particle out of the trap in the radial direction. Newton's equations of motion in Cartesian coordinates are as follows:

$$\begin{aligned} \frac{\mathrm{d}^2x}{\mathrm{d}t^2} - \omega_\mathrm{c}\frac{\mathrm{d}y}{\mathrm{d}t} - \frac{1}{2}\omega_\mathrm{z}^2 x = 0, \\ \frac{\mathrm{d}^2y}{\mathrm{d}t^2} + \omega_\mathrm{c}\frac{\mathrm{d}x}{\mathrm{d}t} - \frac{1}{2}\omega_\mathrm{z}^2 y = 0, \\ \frac{\mathrm{d}^2z}{\mathrm{d}t^2} + \omega_\mathrm{z}^2 z = 0, \end{aligned} \tag{1.24}$$

where

$$\omega_z = \sqrt{\frac{2QU_0}{Md^2}}. \tag{1.25}$$

The motion in $z$-direction is a simple harmonic oscillation with an axial frequency $\omega_\mathrm{z}$ decoupled from the transverse motion in the $x$- and $y$-directions.

To describe the motion in the $x, y$-plane we introduce the complex variable $u = x + \mathrm{i}y$. The radial equations of motion then reduce to

$$\frac{\mathrm{d}^2u}{\mathrm{d}t^2} + \mathrm{i}\omega_\mathrm{c}\frac{\mathrm{d}u}{\mathrm{d}t} - \frac{1}{2}\omega_\mathrm{z}^2 u = 0. \tag{1.26}$$

The general solution is found by setting $u = \exp(-\mathrm{i}\omega t)$ to obtain the algebraic condition

$$\omega^2 - \omega_\mathrm{c}\omega + \frac{1}{2}\omega_\mathrm{z}^2 = 0. \tag{1.27}$$

Then the general solution is given by

$$u(t) = R_+ \exp[-\mathrm{i}(\omega_+ t + \alpha_+)] + R_- \exp[\mathrm{i}(\omega_- t + \alpha_-)], \tag{1.28}$$

with

$$\omega_+ = \frac{1}{2}(\omega_\mathrm{c} + \sqrt{\omega_\mathrm{c}^2 - 2\omega_\mathrm{z}^2}), \quad \omega_- = \frac{1}{2}(\omega_\mathrm{c} - \sqrt{\omega_\mathrm{c}^2 - 2\omega_\mathrm{z}^2}),$$

the modified cyclotron frequency and the magnetron frequency, respectively. Here $R_+$, $R_-$, $\alpha_+$, and $\alpha_-$ are the radii and the phases of the respective motions, determined by the initial conditions. The relation (1.28) is the equation of an epicycloid. Figure 1.9 shows a sketch of the ion trajectory in all three dimensions. It describes a trajectory around the trap center where the particle moves within a circular strip between an outer radius $R_+ + R_-$ and an inner radius $|R_+ - R_-|$. In order that the motion be bounded the roots of (1.29) must be real, leading to the trapping condition

$$\omega_\mathrm{c}^2 - 2\omega_\mathrm{z}^2 > 0, \tag{1.29}$$

or equivalently

$$\frac{|Q|}{M}B_0^2 > \frac{4|U_0|}{d^2}, \quad QU_0 > 0. \tag{1.30}$$

Several useful relations exist between the eigenfrequencies of the trapped particle:

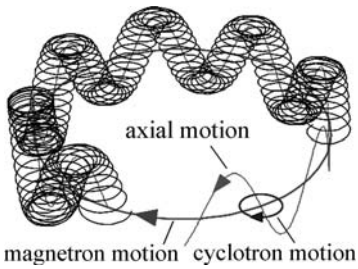


**Fig. 1.9.** Sketch of the ion trajectory in a Penning trap

$$\omega_+ + \omega_- = \omega_c, \tag{1.31}$$

$$2\omega_+\omega_- = \omega_z^2, \tag{1.32}$$

$$\omega_+^2 + \omega_-^2 + \omega_z^2 = \omega_c^2. \tag{1.33}$$

The last is known as "invariance theorem" since the first-order frequency shifts by trap imperfections cancel [16].

### 1.2.2 Motional Spectrum in Penning Traps

The motional spectrum of an ion in a Penning trap contains the fundamental frequencies $\omega_+$, $\omega_-$ and $\omega_z$ as shown in the solution of the equations of motion. These frequencies can be measured using resonant excitation of the ion motion by applying an additional dipole rf field to the trap electrodes. An indication of resonant excitation is a rapid loss of stored ions due to the gain in energy from the rf field, which enables them to escape. The electrostatic field inside the trap is expected to be a superposition of many multipole components, hence many combinations of the fundamental frequencies and their harmonics become visible, depending on the amplitude of the exciting field. Figure 1.10 shows the number of trapped electrons as a function of the frequency of an excitation rf field which enters the apparatus by an antenna placed near the trap. Identification of the resonances is through their different dependence on

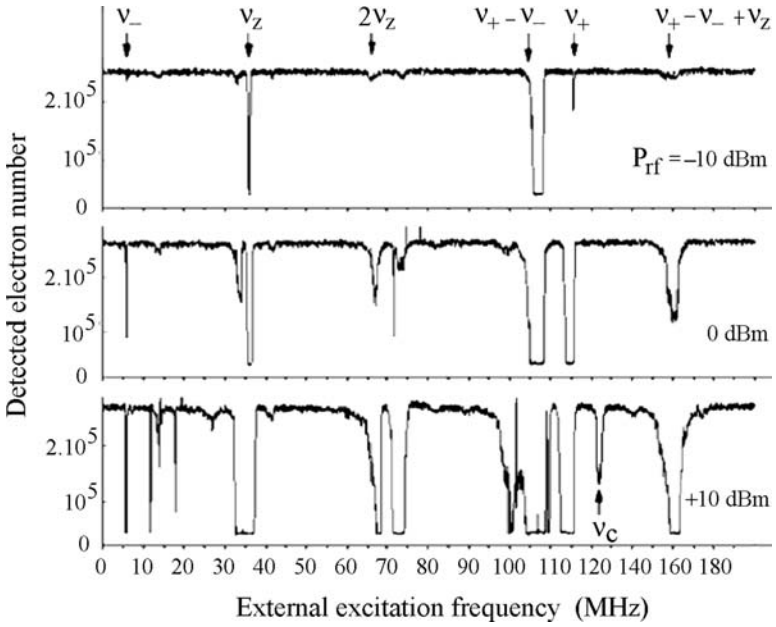


**Fig. 1.10.** Observed motional resonances of electrons in a Penning trap taken at different amplitudes of an exciting rf field

the electrostatic field strength. The axial frequency $\omega_z$ depends on the square root of the trapping voltage while $\omega_+$ and $\omega_-$ vary linearly with the voltage. Of particular interest is the combination $\omega_+ + \omega_-$, since it is independent of the trapping voltage, and equals the cyclotron frequency of the free ion $\omega_c$ whose measurement can serve to calibrate the magnetic field at the ion position.

The frequency $\omega_c$ can be obtained in three different ways: Direct excitation of the sideband $\omega_+ + \omega_-$, measurement of the fundamental frequency $\omega_+$ at different trapping voltages $U_0$ and extrapolating to $U_0 = 0$, or using the relation (1.33). The last is particularly useful since it is, to first-order, independent of perturbations arising from field imperfections, as stated earlier [16].

### 1.2.3 Penning Trap Imperfections

As in the case of Paul traps, in real Penning traps the conditions are considerably more complicated than the ideal description in Sect. 1.2.2. The hyperbolic surfaces are truncated and may deviate from the ideal shape, the trap axis may be tilted with respect to the direction of the magnetic field, and the long range Coulomb potential of ions adds to the trapping potential when more than a single ion is trapped. The departures of the field from the pure quadrupole introduce nonlinearity in the equations of motion, and coupling between the degrees of freedom. The main effects of these imperfections on the behavior of the trapped ions are a shift in the eigenfrequencies and reduction in the storage capability of the trap.

*Electric field imperfections.* As in the case of the previously discussed Paul trap, imperfections in the electrostatic field can be treated by a multipole expansion of the potential with coefficients $c_n$ characterizing the strength of higher order components in the trapping potential as stated in (1.19). Several authors [17–20] have calculated the resulting shift in the ion oscillation frequency. Assuming that due to rotation and mirror symmetry of the trap only even orders contribute and regarding the octupole term ($c_4$) as the most important contribution the results are

$$\begin{aligned}
\Delta\omega_z &= \frac{3}{4}\,\frac{c_4}{d^2}\,\omega_z\,[R_z^2 - 2(R_+^2 + R_-^2)],\\
\Delta\omega_+ &= \frac{3}{4}\,\frac{c_4}{d^2}\,\frac{\omega_z^2}{\omega_+ - \omega_-}\,(R_+^2 + 2R_-^2 - 2R_z^2),\\
\Delta\omega_- &= -\frac{3}{2}\,\frac{c_4}{d^2}\,\frac{\omega_z^2}{\omega_+ - \omega_-}\,(R_-^2 + 2R_+^2 - 2R_z^2).
\end{aligned} \tag{1.34}$$

To minimize these shifts, it is obviously necessary not only to make the trap as perfect as possible but also to reduce the oscillation amplitude $R$ by some ion cooling method.

*Magnetic field inhomogeneities.* An inhomogeneity in the superimposed magnetic field $B_0$ of the Penning trap also leads to a shift of the field-dependent frequencies. As in the electric field case, a magnetostatic field in

a current-free region can be derived from a potential function $\Phi_{\mathrm{m}}$, which can be expanded in the following multipole series:

$$\Phi_{\mathrm{m}} = B_0 \sum_{n=0}^{\infty} b_n \rho^n P_n(\cos\theta). \tag{1.35}$$

In the case of mirror symmetry in the trap's mid plane, the odd coefficients vanish. If we retain only the $b_2$ term in the expansion, the solution of the equations of motion leads to a frequency shift for the most interesting case of the sideband $\omega_+ + \omega_- = \omega_{\mathrm{c}}$ given by

$$\Delta\omega_{\mathrm{c}} = \omega_{\mathrm{c}} \frac{b_2}{2} \left( R_{\mathrm{z}} + \frac{\omega_- R_+ - \omega_+ R_-}{\omega_+ - \omega_-} \right). \tag{1.36}$$

Higher orders are treated in Sect. 3.12.

Other imperfections such as an ellipticity of the trap or a tilt angle between the trap axis and the magnetic field direction also shift the eigenfrequencies. It should be noted, however, that these shifts do not affect the free ion cyclotron frequency $\omega_{\mathrm{c}}$ in first-order when using the *invariance theorem* $\omega_{\mathrm{c}}^2 = \omega_+^2 + \omega_-^2 + \omega_{\mathrm{z}}^2$ [16].

*Space charge shift.* The space charge potential of a trapped ion cloud also shifts the eigenfrequencies of individual ions. From a simple model of a homogeneous charge density in the cloud, we are led to a decrease in the axial frequency proportional to the square root of the ion number. This has been verified experimentally (Fig. 1.11).

More important for high-precision spectroscopy is the space charge shift in the frequencies when we are dealing with small numbers of ions, where the simple model is no longer adequate. The observed shift depends on the mean inter-ion distance and consequently on the ion temperature. For ions cooled to 4 K, Van Dyck et al. [21] have observed shifts of opposite signs in the perturbed cyclotron and magnetron frequencies, amounting to 0.5 ppb per stored ion. The shift increases approximately linearly with the charge of the ions. The electrostatic origin of the shifts suggests that the sum of the

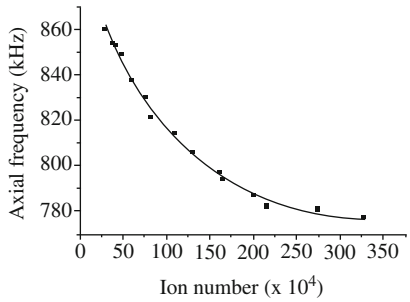


**Fig. 1.11.** Shift of the axial frequency as function of the trapped ion number

perturbed cyclotron and magnetron frequencies, which equals the free ion cyclotron frequency, should be independent of the ion number. In fact, the shifts observed in the sideband $\omega_+ + \omega_- = \omega_c$ are consistent with zero.

*Image charges.* An ion oscillating with amplitude $r$ induces in the trap electrodes image charges which create an electric field that reacts on the stored ion and shifts its motional frequencies. The shift has been calculated by Van Dyck et al. [21] using a simple model. If the trap is replaced by a conducting spherical shell of radius $a$, the image charge creates an electric field given by

$$\boldsymbol{E} = \frac{1}{4\pi\varepsilon_0}\frac{Qa}{(a^2 - r^2)^2}\boldsymbol{r}. \tag{1.37}$$

Since this field is added to the trap field, it causes a shift in the axial frequency amounting to

$$\Delta\omega_z = -\frac{1}{4\pi\varepsilon_0}\frac{Q^2}{2Ma^3\omega_z}, \tag{1.38}$$

and like $E$ scales linearly with the ion number $n$, being significant only for small trap sizes. Since it is of purely electrostatic origin, the electric field-independent combination frequency $\omega_+ + \omega_- = \omega_c$ is not affected.

*Instabilities of the ion motion.* Another consequence of the presence of higher order multipoles in the field is that ion orbit instability can occur at certain operating points, where it would otherwise be stable in a perfect quadrupole field. Using perturbation theory to solve the equations of motions when the trap potential is written as a series expansion in spherical harmonics, Kretzschmar [17] has shown that the solution exhibits singularities for operating points at which

$$n_+\omega_+ + n_-\omega_- + n_z\omega_z = 0, \tag{1.39}$$

where $n_+, n_-, n_z$ are integers. The ion trajectory at such points is unstable and the ion is lost from the trap. In Fig. 1.12 the results of measurements obtained for different trap voltages at a fixed value of the magnetic field, on a cloud of trapped electrons are shown. The combined effect of space charge and trap imperfections leads to the loss of the particles [22]. The observed instabilities which become more discernible for extended storage times, can be assigned to operating conditions predicted from (1.39). These results show that in practice it is very difficult to obtain stable operating conditions when the trapping voltage exceeds about half the value allowed by the stability criterion.

### 1.2.4 Storage Time

Ideally a stored ion would remain in a Penning trap for unlimited time. As discussed earlier, trap imperfections, however, may lead to ion loss. Proper choice of the operating conditions and reduced ion oscillation amplitude by ion cooling makes this negligible. The limiting factor then would be collisions

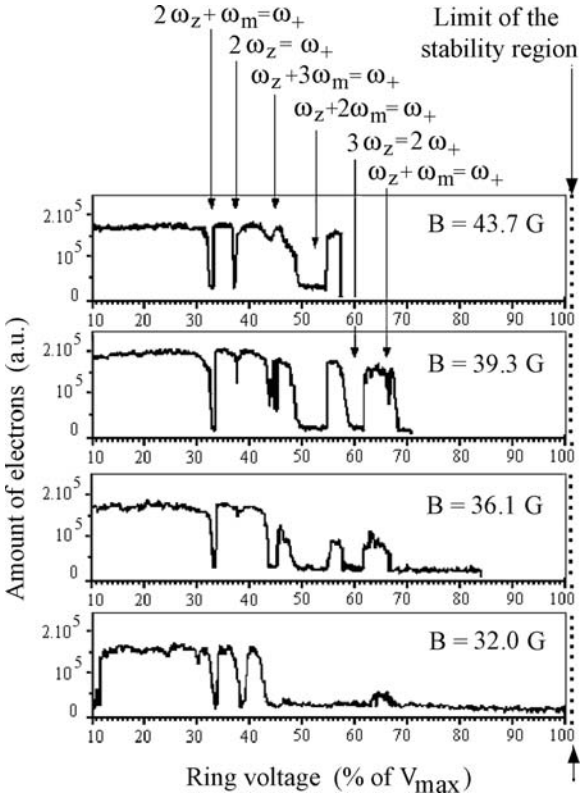


**Fig. 1.12.** Observed number of trapped electrons vs. trapping potential at different magnetic field strengths. The trap voltage is given in units of the maximum voltage as derived from (1.29). The combinations of eigenfrequencies leading to trap instabilities according to (1.39) is indicated [22]

with neutral background molecules, since they cause an increase in the magnetron orbit of the ion which will eventually hit the trap boundary. Typical storage times at $10^{-8}$ Pa are several minutes and at extremely low pressures of below $10^{-14}$ Pa, obtained by cryopumping, storage times of many months are obtained. The problem of collision-induced increase of the magnetron orbit can be overcome by an additional rf field at the sum frequency of the perturbed cyclotron and the magnetron motions [23]. The field is applied between adjacent segments of the ring electrode of the Penning trap, which is split into four quadrants. The effect of this field is to couple the two motions. The cyclotron motion is damped by collisions with background atoms and the coupling transfers the damping to the magnetron motion. The net effect is that the ions aggregate near the trap center and consequently the storage time is extended [24].

### 1.2.5 Storage Capability

The limiting ability to trap charged particles in a Penning type of trap is determined by their mutual electrostatic repulsion. From the condition for stable confinement which gives in effect the magnetic field required to balance the radial component of the electric field, we can find a value for the limit on the number density of ions that can be trapped at a given magnetic field intensity. This limit, sometimes called the Brillouin limit, is given by

$$n_{\lim} = \frac{B^2}{2\mu_0 Mc^2}, \tag{1.40}$$

where $\mu_0$ is the permeability of free space. Naturally, as this limit is approached, the individual particle picture is no longer valid; one is dealing with a plasma.

### 1.2.6 Spatial Distribution

As in the Paul trap, an ion cloud in thermal equilibrium in a Penning trap assumes a Gaussian density distribution. The width of the distribution, however, can be changed by a technique introduced in 1977 at the University of California at San Diego and called the "rotating wall": The crossed electric and magnetic fields of a Penning trap causes a charged particle to rotate around the trap center at the magnetron frequency [25]. In addition, the cloud may be forced to rotate at different frequencies by an external torque from an electric field rotating around the symmetry axis. The ring electrode of a Penning trap is split into different segments. A sinusoidal voltage $V_{wj}$ of frequency $\omega_w$ is applied to the segments at $\theta_j = 2\pi j/n$, where $n$ is the number of segments, with $V_{wj} = A_w \cos[m(\theta_j - \omega_w t)]$. Figure 1.13 illustrates an eight-segment configuration.

The additional centrifugal force from the plasma rotation leads to a change in plasma density and spatial profile. Thus, variation of the rotating wall frequency allows the plasma to be compressed or expanded if the field is rotating with or against the rotation of the plasma, respectively (Fig. 1.14).

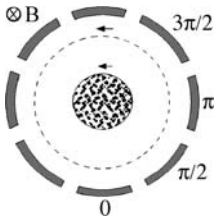


**Fig. 1.13.** Ring electrode of a trap in an eight-segment configuration for application of a rotating electric field

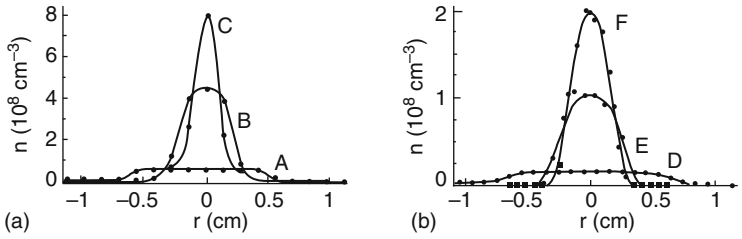


**Fig. 1.14.** Measured change of density by application of rotating wall field on an electron (**a**) and $Be^+$ (**b**) plasma. B, E: No rotating field, A, D: Rotating field opposite to magnetron motion, C, F: Field rotating in direction of the magnetron motion [26]

## 1.3 Trap Techniques

### 1.3.1 Trap Loading

#### In-trap Ion Creation

The easiest way to load ions into the trap is to create them inside the trapping volume by photon or electron ionisation of an atomic beam or the neutral background gas. At room temperature the energy of the ions is in general significantly smaller than the trap potential depth and all ions are confined. Alternatively the ions can be created by surface ionisation from a filament placed at the edge of the trapping volume (Fig. 1.15). Atoms of interest can be deposited on the filament's surface or injected as ions into the material. Heating the filament releases ions from the surface. The efficiency depends on the work function of the filament's material and the ionisation potential of the atom under investigation. Using filaments of Pt, W, or Rh with high workfunctions and atoms like Ba, Sr, Ca with low ionisation potentials, typical efficiencies are of the order of $10^{-5}$.

#### Ion Injection from Outside

An ion injected into a Penning trap from an outside source under high-vacuum condition may be captured by proper switching of the trap electrodes: When the ion travels along the magnetic field lines and approaches the first end cap electrode, its potential is set to zero while the second end cap is held at some retarding potential. If the axial energy of the ion is smaller than the retarding potential, it will be reflected. Before the ion leaves the trap through the first end cap, its potential is raised and prevents the ion from escaping (Fig. 1.16).

This simple method requires that the arrival time of the ion at the trap is known; this is achieved by pulsing the ion source. Moreover, the switching has to be performed in a time shorter than twice the transit time of the ions through the trap. For ion kinetic energies of a few 100 eV and a trap size of

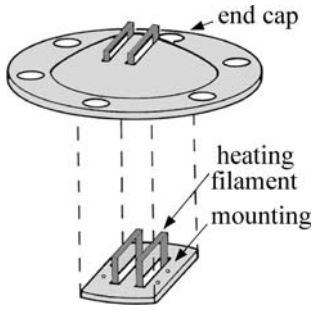


**Fig. 1.15.** Filaments for ion production by surface ionisation placed in a slot of a traps end cap electrode

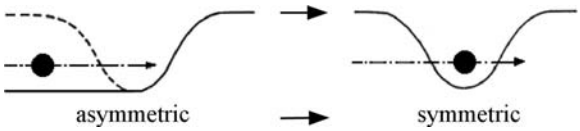


**Fig. 1.16.** Simple model describing the ion capture in a Penning trap

1 cm this time is of the order of 100 ns. Successful capture of ions from a pulsed source is routinely used at the ISOLDE-facility at CERN, where nearly 100% efficiencies are achieved [27].

Injection into a Paul trap under similar conditions is more difficult, since the time varying trapping potential of typically a megaherz frequency cannot be switched from zero to full amplitude in a time of the order of less than a microsecond. The ion longitudinal kinetic energy, however, may be transferred into transverse components by the inhomogeneous electric trapping field and thus the ions may be confined for some finite time. Schuessler and Chun-sing [28] have made extensive simulations and phase considerations and have found that ions injected at low energy during a short interval when the ac trapping field has zero amplitude may remain in the trap for some finite time.

The situation is different when the ions undergo a loss in kinetic energy while they pass through the trap. This energy loss is most easily obtained by collisions with a light buffer gas. The density of the buffer gas has to be at least of such a value that the mean free path of the ions between collisions is of the trap's size. Coutandin et al. [29] have shown that the trap is filled up to its maximum capacity in a short time at pressures around $10^{-3}$ Pa in a 1 cm size Paul trap when ions are injected along the trap axis with a few kiloelectronvolts kinetic energy (Fig. 1.17). The same method is used routinely in many experiments where a high-energy ion beam is delivered from an accelerator. It is stopped and cooled by buffer gas collisions in a gas filled linear rf trap and then ejected at low energies with small energy spread into a trap operated at ultra-high vacuum for further experiments [30]. Injection into a Penning trap using collisions to entrap them requires some care. The ion's

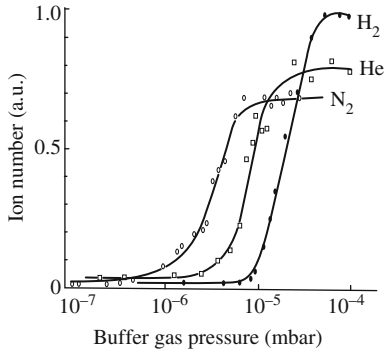


**Fig. 1.17.** Trapped $Ba^+$ ion number vs. buffer gas pressure for He, $H_2$, and $N_2$ when injected at a few kiloelectronvolts kinetic energy. The maximum ion number for $H_2$ is arbitrarily set to 1 [29]

motion becomes unstable since collisions lead to an increase of the magnetron radius. This can be overcome, as described earlier, if the trap ring electrode is split into four segments and an additional rf field is applied between adjacent parts to create a quadrupolar rf field in the radial plane. At the sum of the perturbed cyclotron frequency $\omega_+$ and the magnetron frequency $\omega_-$ this field couples the two oscillations. The damping of the cyclotron motion by collisions with the background atoms, overcomes the increase of the magnetron radius and as a result the ions aggregate near the trap's center [23]. Since $\omega_+ + \omega_- = \omega_c$, the free ion cyclotron frequency depends on the ion mass, it is possible to stabilize a particular isotope or even isobar in the trap by proper choice of the rf frequency [31] while ions of unwanted mass do not remain in the trap.

### 1.3.2 Trapped Particle Detection

#### Destructive Detection

*Paul traps.* Ions confined in a Paul trap may leave the trap either by lowering the potential of one end cap electrode or by application of a voltage pulse of high amplitude. They can be counted by suitable detectors such as ion multiplier tubes or channel plate detectors. By different arrival times to the detector, ions of different charge-to-mass ratio can be distinguished (Fig. 1.18). The amplitude of the detector pulse depends on the phase of the leading edge of the ejection pulse with respect to the phase of the rf trapping voltage.

When several ion species are simultaneously trapped, a particle of specific charge-to-mass ratio can be selectively ejected from the trap and counted by a detector if an rf field resonant with the axial oscillation frequency of the ion of interest is applied in a dipolar mode between the trap's end cap electrodes [32].

*Penning traps.* Ions can be released from the Penning trap, generally placed in the most homogeneous part of a (superconducting) solenoid, by switching

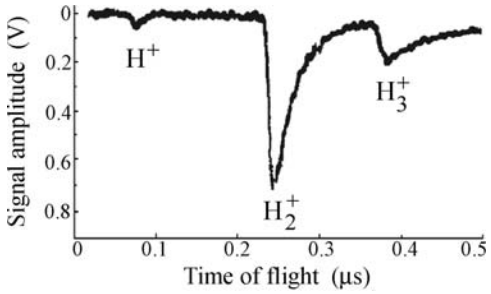


**Fig. 1.18.** Ejection of simultaneously trapped $H^+$, $H_2^+$, and $H_3^+$ ions from a Paul trap and detection by an ion multiplier located 5 cm from the traps end cap [14]

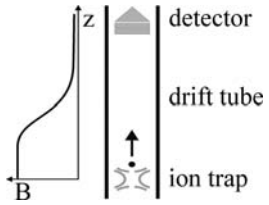


**Fig. 1.19.** Time-of-flight detection of ions released from a Penning trap. The magnetic field points in the vertical direction

one of the end cap potentials to zero. The particles then travel along the magnetic field lines until they arrive at a detector outside the magnetic field region (Fig. 1.19). With finite radial kinetic energies the ions have some angular momentum which has associated with it an orbital magnetic moment $\mu$. In the fringing field of the magnet a force $\boldsymbol{F} = \boldsymbol{\nabla}(\mu B)$ acts upon the ions and accelerates them onto the detector. The time-of-flight for a given angular momentum is determined by the ion's mass and thus the different masses of simultaneously trapped ions can be distinguished. We note that the excitation of the radial motion by an additional rf field increases the angular momentum and thus leads to a reduced time-of-flight. This method of detecting ion oscillation frequencies, particularly the cyclotron frequency, serves as the basis for many high-precision mass spectrometers [33].

### Nondestructive Detection

*Tank circuit damping.* The mass dependent oscillation frequencies of ions in a trap can be used for detection without ion loss. A tank circuit consisting of an inductance L connected in parallel with the trap electrodes as capacitance C is weakly excited at its resonance frequency $\omega_{\mathrm{LC}}$ (Fig. 1.20). The ions' axial oscillation frequency $\omega_{\mathrm{z}}$ can be changed by variation of the electric trapping field. When the frequencies are tuned to resonance, energy is transferred from the LC circuit to the ions leading to a damping of the circuit, and a decrease

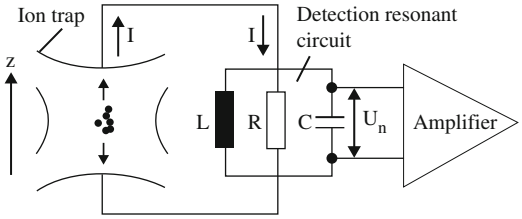


**Fig. 1.20.** Electronic circuit for nondestructive detection of trapped ion clouds

of the voltage across it. Modulation of the trap voltage around the operating point at which resonance occurs and rectification of the voltage across the circuit lead to a repeated voltage drop, whose amplitude is proportional to the number of trapped ions. When different ions are simultaneously confined signals appear at different values of the modulated trapping voltage. The sensitivity of the method depends on the quality factor $\tilde{Q}$ of the resonance circuit. With moderate values of the order of $\tilde{Q} = 50$ about 1,000 trapped ions lead to an observable signal.

*Bolometric detection.* In the bolometric detection of trapped ions, first proposed and realised by Dehmelt and co-workers [34–36] the ions are kept in resonance with a tuned LC circuit connected to the trap electrodes in a way similar to what was discussed in the previous section. An ion of charge $Q$ oscillating between the end cap electrodes of a trap induces a current in the external circuit given by

$$I = \Gamma Q\dot{z}/(2z_0), \tag{1.41}$$

where $2z_0$ is the separation of the end caps, and $\Gamma$ is a correction factor, which accounts for the approximation of the trap electrodes by parallel plates of infinite dimension. For hyperbolically shaped electrodes $\Gamma \simeq 0.75$. The electromagnetic energy associated with this current will be dissipated as thermal energy in the parallel resonance resistance of the LC circuit, $R$. The increased temperature $T$ of that resistance results in an increased thermal noise voltage $U_{\text{noise}}$ in a bandwidth $\delta\nu$:

$$U_{\text{noise}} = \sqrt{4kTR\delta\nu}. \tag{1.42}$$

If the number of stored ions is known, the noise voltage measured by a narrow band amplifier can serve as a measure of the ion temperature. When ions of different charge-to-mass ratios are stored simultaneously their oscillation frequencies can be brought into resonance with the circuit by sweeping the trap voltage. Each time an ion species is resonant with the circuit, the noise amplitude increases and can be detected. An example is shown in Fig. 1.21 where the increased noise of the axial resonances of different highly charged ions in a Penning trap is recorded. For high sensitivity the thermal noise power of the circuit has to be kept as low as possible. When superconducting circuits at temperatures around 4 K are used, single ions can be well observed.

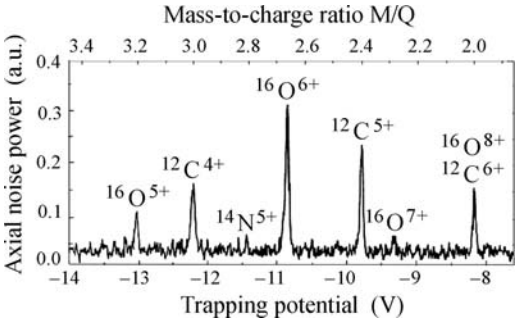


**Fig. 1.21.** Thermal noise induced in an LC circuit by simultaneously trapped ions of different charge-to-mass ratios in a Penning trap [37]

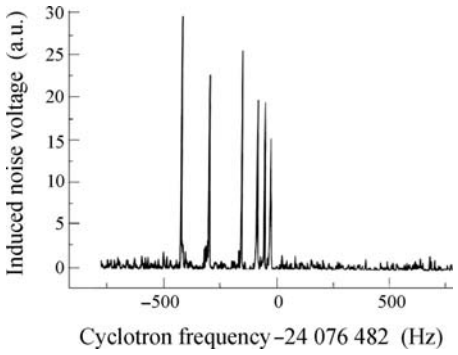


**Fig. 1.22.** Fourier transform of the noise from $C^{5+}$ ions induced in a tank circuit attached to two segments of the ring electrode of a Penning trap. The $\tilde{Q}$ value of the circuit was 4,000. The magnetic field was inhomogeneous and ions located at different places in the trap have slightly different cyclotron frequencies [37]

*Fourier transform detection.* A Fourier transform of the noise induced by the oscillating ions in a tank circuit shows maxima at the ion oscillation frequencies. When superconducting circuits with quality factors $\tilde{Q}$ of several thousands are used the signal strength from a single ion is sufficient for detection. Figure 1.22 shows the noise induced by six ions in a circuit attached to two segments of the ring electrode of a Penning trap. The magnetic field was inhomogeneous and ions located at different places in the trap have slightly different cyclotron frequencies.

When the ions are kept continuously in resonance with the tank circuit, the increased thermal energy of the detection circuit, due to the induced ion currents, will be dissipated [38]. Consequently, the ion oscillation will be exponentially damped with a time constant $\tau$ given by

$$\tau = \frac{(2z_0)^2}{\Gamma^2 R} \frac{M}{Q^2}, \tag{1.43}$$

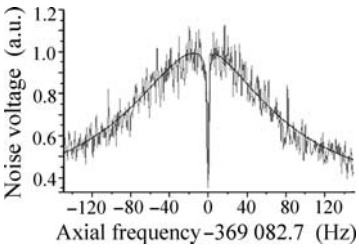


**Fig. 1.23.** Fourier transform of the noise of a superconducting axial resonance circuit in the presence of a single trapped $C^{5+}$ ion in thermal equilibrium with the circuit. The sum of the circuit's thermal noise and the induced noise from the oscillating ion leads to a minimum at the ion's oscillation frequency [37]

where $R$ is the impedance of the circuit. When the ions reach thermal equilibrium with the circuit, excess noise can no longer be detected; nevertheless, the presence of ions can be detected by a spectral analysis of the circuit noise. The voltage that the ion induces with its remaining oscillation amplitude adds to the thermal noise of the circuit, however with opposite phase. As a result, the total noise voltage at the ion oscillation frequency is reduced, and the spectral distribution of the noise shows a minimum at this frequency when ions are present in the trap. This is shown in Fig. 1.23 for a single $C^{5+}$ ion.

*Optical detection.* A very efficient way to detect the presence of ions in the trap is to monitor their laser induced fluorescence. This method is, of course, restricted to ions which have an energy-level scheme which allows excitation by available lasers. It is based on the fact that the lifetime of an excited ionic energy level is of the order of $10^{-7}$ s when it decays by electric dipole radiation. Repetitive excitation of the same ion by a laser at saturation intensity then leads to a fluorescence count rate of $10^7$ photons per second. Of those a fraction of the order of $10^{-3}$ can be detected if we assume a solid angle of $4\pi/10$, a photomultiplier detection efficiency of 10%, and filter and transmission losses of 90%, leading to an easily observable signal (Fig. 1.24).

The method is most effective when the ion under consideration has a large transition probability for the excitation from the electronic ground state as in alkali-like configurations. It becomes particularly easy when the excited state ion falls back directly into the ground state. Such two-level systems are available in $Be^+$ and $Mg^+$ and consequently these ions are preferred subjects when optical detection of single stored particles is studied. For other ions of alkali-like structure such as $Ca^+$, $Sr^+$, or $Ba^+$ it becomes slightly more complicated since the excited state may decay into a long-lived low lying metastable state which prevents fast return of the ion into its ground state; then an additional laser is required to pump the ion out of the metastable state. Signals of the expected strength have been obtained in all those ions. They allow even the visual observation of a single stored ion $Ba^+$ as demonstrated in a pioneering experiment at the University of Heidelberg [40].

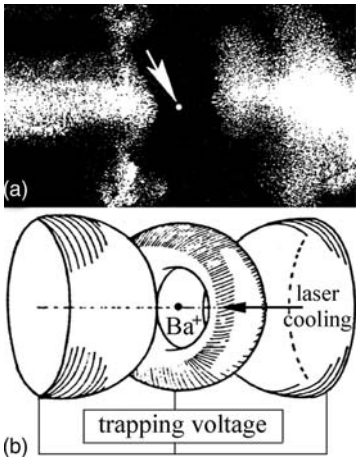


**Fig. 1.24.** The first observation of an atomic particle, as a single $Ba^+$ ion (**a**) trapped in a miniaturized Paul trap (**b**) Reprinted with permission from [39]

## 1.4 Ion Cooling Techniques

The mean kinetic energy of trapped ions depends on the operating conditions of the trap and the initial conditions of the ion motion; in thermal equilibrium a typical value is 1/10 of the maximum potential depth. This is in general much higher than room temperature and might cause significant line shifts and broadening in high-precision spectroscopy. Therefore, a number of methods have been developed to reduce the temperature of the trapped particles.

### 1.4.1 Buffer Gas Cooling

*Paul traps.* The influence of ion collisions with neutral background molecules can be treated by the introduction of a damping term in the equations of motion. Major and Dehmelt [9] have shown that ion cooling appears when the ion mass is larger than that of the background molecule. The equilibrium ion temperature results from a balance between collisional cooling and energy gain from the rf trapping field; it depends on the buffer gas pressure (Fig. 1.25).

The thermalization process in a Paul trap applies to the macromotion of the ions, while the amplitude of the micromotion remains fixed, determined by the amplitude of the electric trapping field at the ion's position. Cutler et al. [11] found that the calculated radial density distribution, averaged over the micromotion, changes from a Gaussian at high temperatures to a spherical one with constant density when the temperature approaches zero (see Fig. 1.7).

*Penning traps.* As in the Paul traps the axial motion of an ion in a Penning trap as well as the cyclotron motion are damped by collisions with neutral molecules. The magnetron oscillation, however, is a motion around an electric

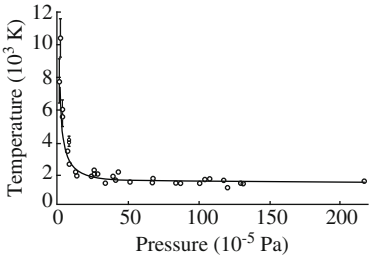


**Fig. 1.25.** Average kinetic energy of $Ca^+$ vs. $N_2$ background gas pressures [41]

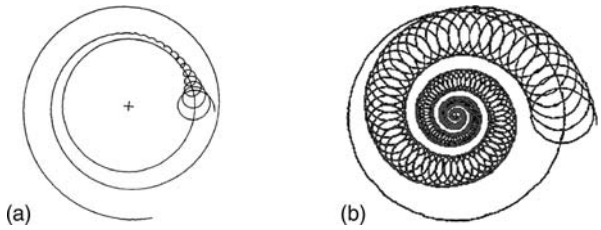


**Fig. 1.26.** Simulation of an ion radial trajectory in a Penning trap under the influence of collisions with neutral molecules (**a**) without and (**b**) with a quadrupolar rf coupling fields at $\omega = \omega_+ + \omega_-$

potential hill and collisions tend to increase the radius of the magnetron orbit until the particle gets lost from the trap. This problem can be overcome by the introduction of an additional transverse quadrupole rf field at the sum of the magnetron and reduced cyclotron frequencies applied between four segments of the ring electrode. It couples the two motions and the leads to an aggregation of the ions near the trap center [19, 23]. Figure 1.26 shows a simulation of the ion trajectory in the radial plane of a Penning trap under the influence of ion–neutral collisions with and without the coupling field. For initial radial amplitudes $R_+^0$ and $R_-^0$ of the two motions, the amplitudes change as

$$R_\pm(t) = R_\pm^0 \exp(\mp\alpha_\pm t), \tag{1.44}$$

with

$$\alpha_\pm = \frac{\gamma}{M}\frac{\omega_\pm}{\omega_+ - \omega_-}. \tag{1.45}$$

### 1.4.2 Resistive Cooling

When an LC-circuit resonant with the ion oscillation frequency is attached between trap electrodes the image currents induced by the ion's motion through the external circuit will increase its thermal energy which will be dissipated to the environment [34–36, 38]. It leads to an exponential energy loss of the ions with a time constant

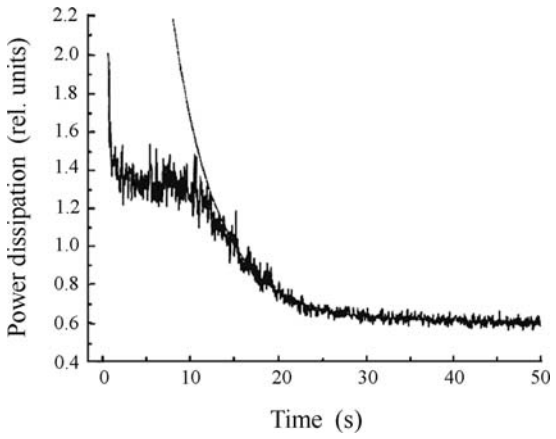


**Fig. 1.27.** Resistive cooling of an ion cloud in a Penning trap monitored by the induced image noise in an attached tank circuit. The center-of-mass (CM) energy is reduced in a short time of about 100 ms while the individual ion oscillation is damped with a much longer time constant (5 s)

$$\tau = \left(\frac{2z_0}{Q}\right)^2 \frac{M}{\omega L}\frac{1}{\tilde{Q}}, \tag{1.46}$$

where $\tilde{Q}$ is the quality factor of the LC circuit. For an electron confined in a trap with $z_0 = 1\,\mathrm{cm}$, a circuit $\tilde{Q} = 100$ with $L = 1\,\mu\mathrm{H}$, oscillating at 300 MHZ we obtain $\tau \simeq 5\,\mathrm{ms}$. The increased time constant for heavier ions can be partly compensated by choosing superconducting circuits with $\tilde{Q}$-values of several thousands. The final ion temperature will be the same as the temperature of the circuit which may be kept in contact with a liquid helium bath at 4 K. Resistive cooling is particularly well suited for Penning traps. In Paul traps the high amplitude of the rf trapping field will in general cause currents through the attached tank circuit which prevents reaching low temperatures.

We note that resistive cooling of an ion cloud affects the center-of-mass (CM) energy only. Coulomb interaction transfers energy from the individual ion oscillation into the CM mode. The rate of this energy transfer depends on the ion number. Thus, two time constants are observed (Fig. 1.27).

### 1.4.3 Laser Cooling

Laser cooling is the most effective way to reduce the ion's kinetic energy. It is based on the conservation of linear momentum in the scattering of many photons from the same ion by repetitive laser excitation. Thus, the basic requirement is that the ion can be excited by electric dipole radiation and the excited state decays rapidly back into the ground state. This is the case in singly ionized Mg and Be ions, which are most often used in laser cooling experiments. Other ions of alkali-like structure such as $Ca^+$, $Sr^+$, $Ba^+$, and

$Hg^+$ have more complex-level schemes but can provide an effective two-level scheme by additional lasers.

*Doppler cooling.* When a laser is tuned in frequency slightly below a resonance transition of an ion only those ions absorb laser light with high probability which move against the direction of the laser beam, because the laser's frequency is Doppler shifted into resonance. During photon absorption, momentum conservation requires the ion to lose momentum. However, the absorbed photon is reemitted with an angular distribution having zero average photon recoil momentum. The net effect is a reduction of ion momentum. To cool stored ions, the laser frequency is swept from low frequency toward the resonance center. As soon as the laser frequency is higher than the ion's resonace frequency the opposite effect occurs: Ions moving in the direction of the laser beam absorb photons and gain energy. As a result the ion cloud expands and the spatial overlap with the laser is reduced. When the fluorescence from the ion cloud is monitored the resonance lineshape becomes asymmetric showing a sharp edge at the high-frequency side (Fig. 1.28a). The rate at which energy is lost depends on the laser detuning from resonance $\delta\omega$, the transition matrix element $P$, the ion's mass $M$, and the laser intensity. The lowest temperature $T_{\min}$ is reached when the Doppler width of the transition is equal to the natural line width ("Doppler limit"):

$$T_{\min} = \frac{\hbar\gamma}{2k_{\mathrm{B}}}, \tag{1.47}$$

where $\gamma$ is the decay rate of the excited state and $k_{\mathrm{B}}$ is the Boltzmann constant. Typical values for $T_{\min}$ are in the millikelvin range. When during the cooling process the temperature becomes so low that the ratio $\Gamma$ between the Coulomb repulsion energy between ions of average distance $a$ and the thermal energy $k_{\mathrm{B}}T/2$

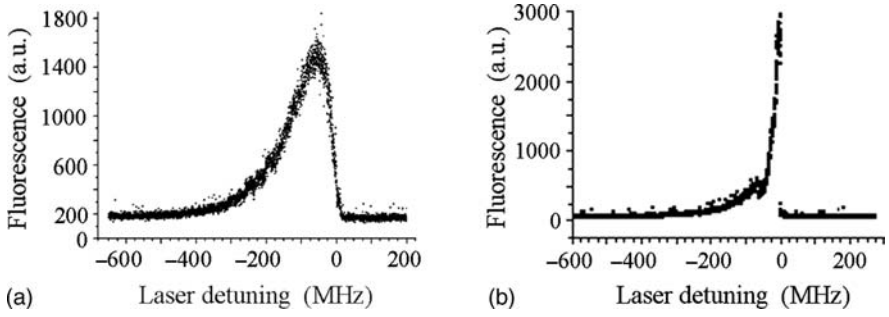


**Fig. 1.28.** Fluorescence from a small cloud of $Ca^+$ ions in a Paul trap when the laser frequency is slowly swept across the $4S_{1/2} - 4P_{1/2}$ resonance. At laser frequencies below resonance ($\Delta\nu < 600\,\mathrm{MHz}$) ions are cooled, above resonance they are heated and the cloud expands. (**a**) Low laser power, (**b**) high-laser power

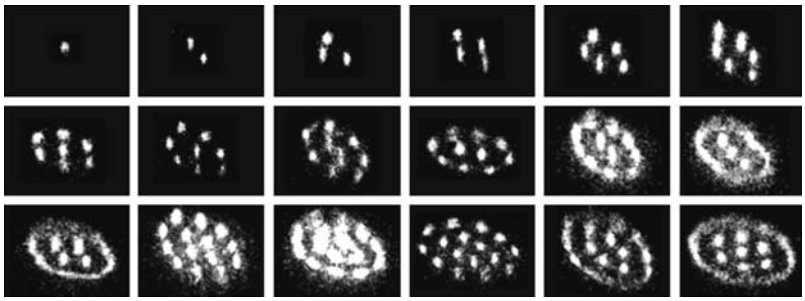

**Fig. 1.29.** Crystalline structures of small $Ca^+$ ion clouds observed by a CCD camera [42]

$$\Gamma = \frac{1}{4\pi\varepsilon_0}\frac{Q^2}{ak_\mathrm{B}T} \tag{1.48}$$

becomes larger than 175, a phase transition to a crystalline structure appears in the ion cloud. It manifests itself by a kink in the fluorescence lineshape, caused by a sudden reduction of the Doppler broadening (Fig. 1.28b). The crystalline structures can be observed directly by a CCD camera (Fig. 1.29).

*Sideband cooling.* When the amplitude of the ion oscillation in the harmonic trap potential becomes smaller than the wavelength of the exciting laser no Doppler broadening appears. Instead distinct sidebands in the excitation spectrum at multiples of the oscillation frequency show up ("Dicke effect"). The requirement is expressed by the condition $\eta << 1$, where $\eta$ is the Lamb–Dicke parameter

$$\eta = k\left(\frac{\hbar}{2M\omega}\right)^{1/2} = \left(\frac{\omega_\mathrm{rec}}{\omega}\right)^{1/2}. \tag{1.49}$$

Here $k$ is the wave number of the laser radiation, $\omega$ the ion oscillation frequency, and $\hbar\omega_\mathrm{rec}$ is the photon recoil energy. The sidebands are resolved when the spontaneous transition rate $\gamma$ is small compared to $\omega/2\pi$. This is in general the case only when transitions to long-lived metastable states are excited. An example is shown in Fig. 1.30. If one irradiates the ion with a narrow band laser tuned to the first lower sideband at $\omega_0 - \omega_\nu$, where $\omega_0$ is the resonance frequency of the ion at rest and $\omega_\nu$ is the oscillation frequency, it absorbs photons of energy $\hbar(\omega_0 - \omega_\nu)$. The reemitted energy is symmetrically distributed among carrier and sidebands, thus amounts on average to $\hbar\omega_0$. Hence, on the average each scattered photon reduced the ions vibrational energy by $\hbar\omega_\nu$ or, in a quantum mechanical picture, reduced the vibrational quantum number $n$ by 1. Continuous excitation on the lower sideband finally drives the ion into the ground state of the confining potential. For a vibrational frequency of 1 MHz this corresponds to a temperature of 50 µK. It is indicated by the disappearance of the lower sideband in the excitation

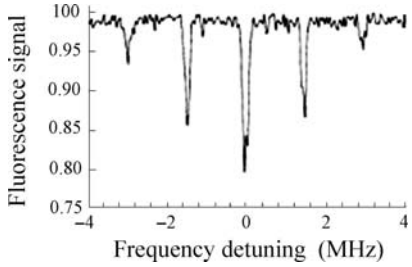


**Fig. 1.30.** Excitation of the $6S_{1/2} - 5D_{5/2}$ quadrupole transition on a single laser cooled $^{198}Hg^{+}$ ion at 282 nm showing a carrier frequency at zero laser detuning from resonance and sidebands at the ions micromotion frequency. Reprinted with permission from [43]

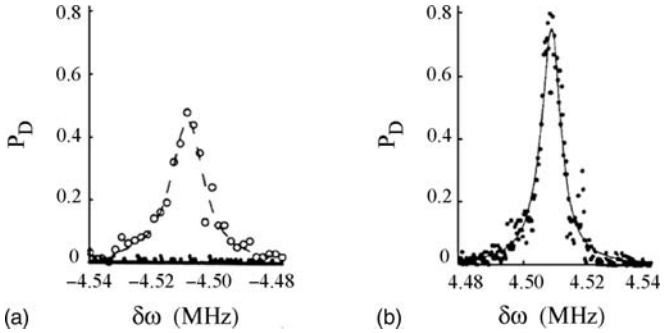


**Fig. 1.31.** Sideband cooling of a single $Ca^{+}$ ion into the vibrational ground state in a Paul trap. The occupation probability $P_D$ of the D-level in the $S_{1/2} - D_{5/2}$ quadrupole transition is plotted vs. the laser detuning $\delta\omega$ after sideband cooling (*full circles*). The lower sideband after Doppler cooling (*open circles*) is shown for comparison. (**a**) First lower sideband; (**b**) first upper sideband [44]

spectrum, because for $n = 0$ no state with $n = -1$ exists in the excited optical level (Fig. 1.31).

### 1.4.4 Radiative Cooling

Accelerated charged particles lose energy by emission of radiation proportional to the square of their acceleration $a$:

$$\frac{\mathrm{d}E}{\mathrm{d}t} = -\frac{Q^2}{4\pi\varepsilon_0 c^3} a^2. \tag{1.50}$$

For a particle oscillating with frequency $\omega$ the mean energy loss is described by

$$\frac{\mathrm{d}E}{\mathrm{d}t} = -\gamma E, \tag{1.51}$$

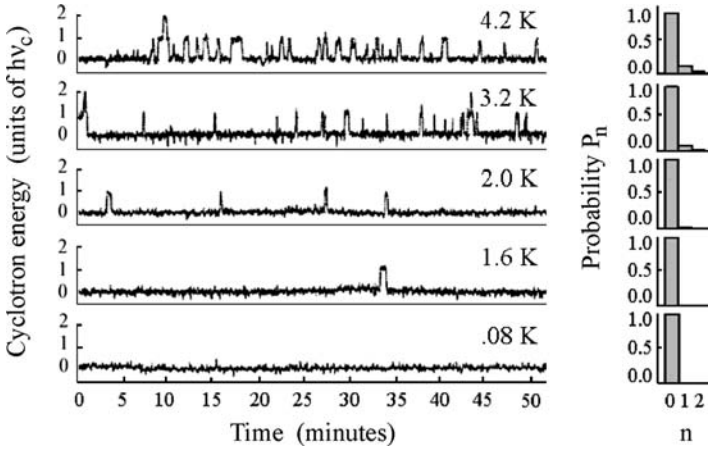


**Fig. 1.32.** Noise power induced in an electrode from a single electron confined in a Penning trap showing the occupation of the lowest quantum states of the cyclotron harmonic oscillator. At $T < 0.1\,\mathrm{K}$ the electron remains in the lowest quantum level for nearly infinitely long times [45]

with the solution

$$E = E_0 \mathrm{e}^{-\gamma t}, \tag{1.52}$$

where

$$\gamma = \frac{1}{6\pi\varepsilon_0}\frac{Q^2\omega^2}{Mc^3}. \tag{1.53}$$

Because of the low mass and the high frequency this energy loss is particularly significant for the cyclotron motion of electrons confined in a Penning trap at high magnetic fields while for atomic ions it can be totally neglected. In a field of 5 T the time constant for electrons is calculated to be $12\,\mathrm{s}^{-1}$. The final temperature is given by the equilibrium with the environment because of excitation by blackbody photons. At cryogenic temperatures the quantum nature of the cyclotron oscillation becomes visible: The probability $P_n$ of the population of a state with quantum number $n$ is given by the Boltzman distribution

$$P_n = A\exp(-n\hbar\omega_\mathrm{c}/k_\mathrm{B}T). \tag{1.54}$$

At $B = 5\,\mathrm{T}$ and a temperature of 100 mK the electron remains almost exclusively in the ground level $n = 0$ of the cyclotron oscillation as experimentally demonstrated Peil and Gabrielse (Fig. 1.32) [45].

http://www.springer.com/978-3-540-92260-5

Charged Particle Traps II
Applications
Werth, G.; Gheorghe, V.N.; Major, F.G.
2009, X, 276 p. 200 illus., 1 illus. in color., Hardcover
ISBN: 978-3-540-92260-5